Supporting Information

Panchromatic Ru(II) Sensitizers Bearing Single Thiocyanate for High Efficiency Dye Sensitized Solar cells

Sheng-Wei Wang,[a] Chun-Cheng Chou,[a] Fa-Chun Hu,[a] Kuan-Lin Wu,[a] Yun Chi,[a,*] John N. Clifford,[b] Emilio Palomares,[b,c] Shih-Hung Liu,[d] Pi-Tai Chou,[d,*] Tzu-Chien Wei[e,*] and Ting-Yun Hsiao[f]

Experimental section

General Procedures. All reactions were performed under nitrogen. Solvents were distilled from appropriate drying agents prior to use. Commercially available reagents were used without further purification. The required azolate ancillaries were synthesized according to the methods documented in literature.[1] All reactions were monitored by TLC with pre-coated silica gel plates (Merck, 0.20 mm with fluorescent indicator UV254). Compounds were visualized with UV irradiation at 254 or 365 nm. Flash column chromatography was carried out using silica gel obtained from Merck (230 - 400 mesh). Mass spectra were obtained on a JEOL SX-102A instrument operating in electron impact (EI) or fast atom bombardment (FAB) mode. ^{1}H and ^{19}F NMR spectra were recorded on a Bruker-400 or INOVA-500 instrument; chemical shifts are quoted with respect to the internal standard tetramethylsilane. Elemental analysis was carried out with a Heraeus CHN-O Rapid Elementary Analyzer. Photophysical data were obtained using an Edinburgh Fluorescence spectrometer FLS928P. Details of the synthetic protocols for the tri-dentate ancillary chelates and the procedures for the DSC cell fabrication and measurement are all given in the electronic supporting information.

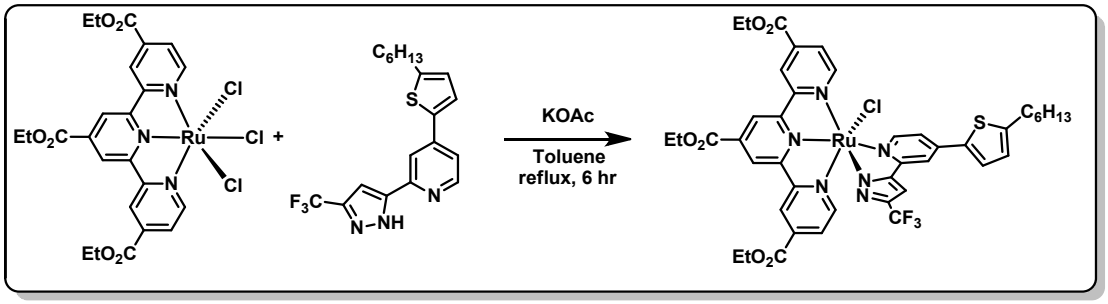

Synthesis of PRT-21-E1

At first, the Ru-precursor was synthesized from 4,4'4''-triethoxycarbonyl-2,2':6',2''-terpyridine (100 mg, 0.2 mmol) and $RuCl_3 \cdot 3H_2O$ (50 mg, 0.2 mmol) by the general procedure.[2] Yield: 110 mg, 83%. After then, a mixture of Ru-precursor (100 mg, 0.15 mmol), 4-(5-hexylthiophen-2-yl)-2-(3-(trifluoromethyl)-1H-pyrazol-5-yl)pyridine[3] (60 mg, 0.16 mmol), and KOAc (30 mg, 0.3 mmol) in 30 mL of toluene was heated to reflux for 6 h. After evaporating the solvent, the residue was purified by silica gel column chromatography (CH_2Cl_2/ethyl acetate = 10:1), yielding **PRT-21-E1** (117 mg, 81%).

Spectral data: ^{1}H NMR (400 MHz, $CDCl_3$, 298 K): δ 9.90 (d, J_{HH} = 6.0 Hz, 1H), 8.82 (s, 2H), 8.70 (s, 2H), 7.98 (d, J_{HH} = 5.6 Hz, 2H), 7.91 (s, 1H), 7.71 (d, J_{HH} = 6.0 Hz, 2H), 7.62 (d, J_{HH} = 4.4 Hz, 1H), 7.56 (d, J_{HH} = 3.6 Hz, 1H), 6.91 (d, J_{HH} = 3.6 Hz, 1H), 6.76 (s, 1H), 4.48 (q, J_{HH} = 7.0 Hz, 2H), 4.39 (q, J_{HH} = 7.0 Hz, 4H), 2.98 (t, J_{HH} = 7.2 Hz, 2H), 1.83 ~ 1.75 (m, 2H), 1.44 ~ 1.27 (m, 15H), 0.93 ~ 0.85 (m, 3H). ^{19}F NMR (376 MHz, $CDCl_3$, 298 K): δ -60.40 (s, 3F).

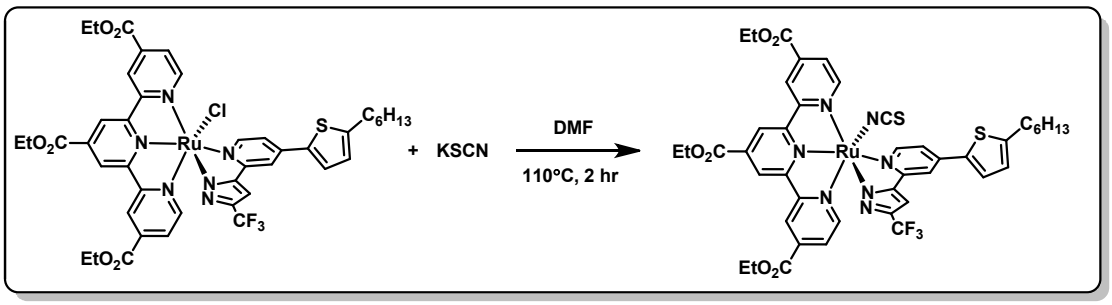

Synthesis of PRT-21-E2

A mixture of **PRT-21-E1** (100 mg, 0.10 mmol) and KSCN (100 mg, 1.0 mmol) in 30 mL of DMF was heated to reflux for 2 h. After evaporating the solvent, the residue

was purified by silica gel column chromatography (CH_2Cl_2/ethyl acetate = 20:1). Yield: **PRT-21-E2** (99 mg, 66%).

Spectral data: ^{1}H NMR (400 MHz, $CDCl_3$, 298 K): δ 9.40 (d, J_{HH} = 6.0 Hz, 1H), 8.81 (s, 2H), 8.69 (s, 2H), 7.92 (d, J_{HH} = 5.8 Hz, 2H), 7.88 (s, 1H), 7.75 (d, J_{HH} = 6.8 Hz, 2H), 7.66 (dd, J_{HH} = 5.8, 2.0 Hz 1H), 7.56 (d, J_{HH} = 3.6 Hz, 1H), 6.92 (d, J_{HH} = 3.6 Hz, 1H), 6.74 (s, 1H), 4.62 (q, J_{HH} = 7.2 Hz, 2H), 4.46 (q, J_{HH} = 7.1 Hz, 4H), 2.92 (t, J_{HH} = 7.4 Hz, 2H), 1.78 ~ 1.72 (m, 2H), 1.59 ~ 1.32 (m, 15H), 0.91 (t, J_{HH} = 6.7 Hz, 3H). ^{19}F NMR (376 MHz, $CDCl_3$, 298 K): δ -60.54 (s, 3F).

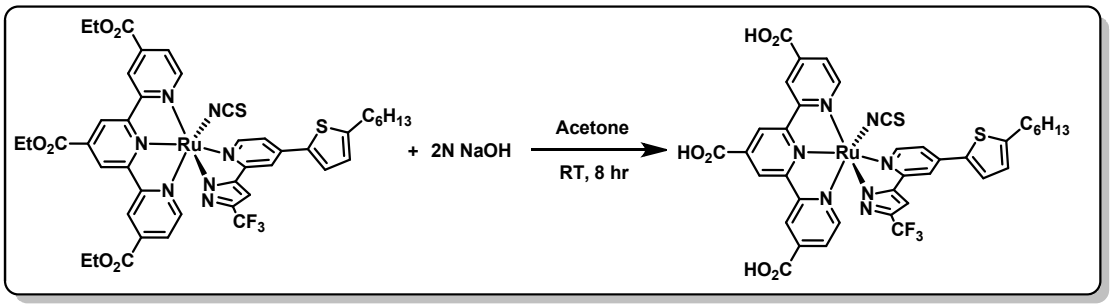

Synthesis of PRT-21

The solid of **PRT-21-E2** (99 mg, 0.10 mmol) was dissolved in a mixture of acetone (30 mL) and 2 M NaOH solution (2 mL) and stirred at room temperature overnight. Finally, the solution was concentrated, and the solid dissolved in 10 mL of H_2O and titrated with 2 N HCl to pH 3 to afford a black precipitate. This black product was washed with H_2O and acetone in sequence, yielding **PRT-21** (70 mg, 78%).

Spectral data of PRT-21: MS (FAB, ^{102}Ru): m/z 903 $(M+1)^+$. ^{1}H NMR (400 MHz, d_6-DMSO, 298 K): δ 9.23 (s, 2H), 9.20 (d, J_{HH} = 6.0 Hz, 1H), 9.09 (s, 2H), 8.43 (s, 1H), 8.05 (d, J_{HH} = 5.6 Hz, 2H), 8.0 (d, J_{HH} = 4.8 Hz, 1H), 7.95 (d, J_{HH} = 3.2 Hz, 1H), 7.76 (s, 1H), 7.84 (d, J_{HH} = 5.6 Hz, 1H), 7.22 (s, 1H), 7.07 (d, J_{HH} = 3.6 Hz, 1H), 2.91(t, J_{HH} = 7.2 Hz, 2H), 1.72 ~ 1.68 (m, 2H), 1.37 ~ 1.29 (m, 6H), 0.87 (t, J_{HH} = 6.8 Hz, 3H). Anal. Calcd for $C_{38}H_{30}F_3N_7O_6RuS_2 \cdot 3H_2O$: C, 47.69; N, 10.25; H, 3.79. Found: C, 48.14; N, 10.36; H, 4.27.

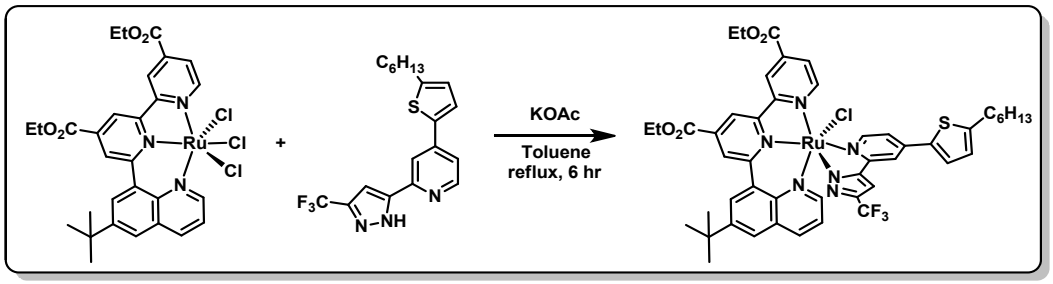

Synthesis of PRT-23-E1

At first, the (Et-Qbpy)$RuCl_3$ was synthesized from diethyl 6-(6-(t-butyl)quinolin-8-yl)-[2,2'-bipyridine]-4,4'-dicarboxylate (Et-Qbpy, 200 mg, 0.4 mmol) and $RuCl_3 \cdot 3H_2O$ (100 mg, 0.4 mmol) by the general procedure.[2] Yield: 240 mg, 84%. After then, a mixture of (Et-Qbpy)$RuCl_3$ (100 mg, 0.14 mmol), 4-(5-hexylthiophen-2-yl)-2-(3-(trifluoromethyl)-1H-pyrazol-5-yl)pyridine[3] (60 mg, 0.16 mmol), and KOAc (30 mg, 0.3 mmol) in 30 mL of toluene was heated to reflux for 6 h. After evaporating the solvent, the residue was purified by silica gel column chromatography (CH_2Cl_2/ethyl acetate = 8:1), yielding **PRT-23-E1** (110 mg, 76%).

Spectral data: ^{1}H NMR (400 MHz, $CDCl_3$, 298 K): δ 9.80 (d, J_{HH} = 6.0 Hz, 1H), 8.79 (s, 1H), 8.71 (s, 1H), 8.56 (s, 1H), 8.55 (s, 1H), 8.46 (s, 1H), 7.96 ~ 7.93 (m, 2H), 7.76 (s, 1H), 7.73 (s, 1H), 7.61 ~ 7.52 (m, 3H), 7.01 (dd, J_{HH} = 8.0, 5.6 Hz, 1H), 6.90 (d, J_{HH} = 3.6 Hz, 1H), 6.56 (s, 1H), 4.55 (q, J_{HH} = 6.8 Hz, 2H), 4.43 (q, J_{HH} = 6.8 Hz, 2H), 2.90 (t, J_{HH} = 7.2 Hz, 2H), 1.76 ~ 1.72 (m, 2H), 1.50 (s, 9H), 1.41 ~ 1.22 (m, 12H), 0.92 ~ 0.81 (m, 3H). ^{19}F NMR (376 MHz, $CDCl_3$, 298 K): δ -60.63 (s, 3F).

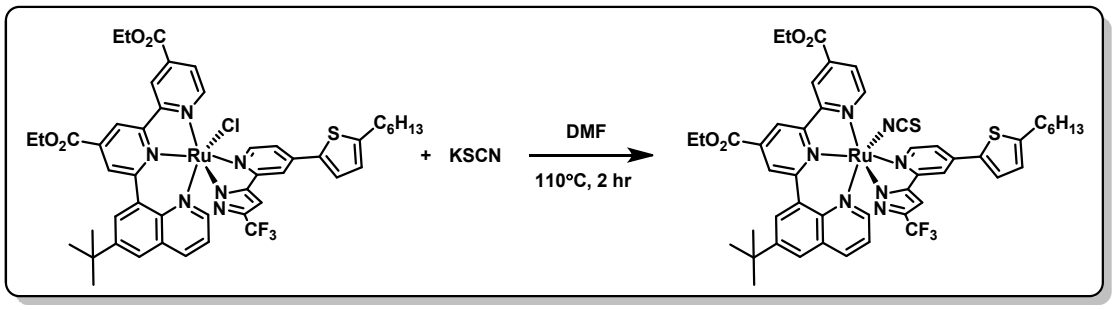

Synthesis of PRT-23-E2

A mixture of **PRT-23-E1** (110 mg, 0.14 mmol) and KSCN (115 mg, 1.2 mmol) in 30 mL of DMF was heated to reflux for 2 h. After evaporating the solvent, the residue was purified by silica gel column chromatography (CH_2Cl_2/ethyl acetate = 10:1),

yielding **PRT-23-E2** (81 mg, 68%).

Spectral data: ^{1}H NMR (400 MHz, d_6-Acetone, 298 K): δ 9.24 (d, J_{HH} = 6.0 Hz, 1H), 9.10 (s, 1H), 9.01 (s, 1H), 8.78 (d, J_{HH} = 2.0 Hz, 1H), 8.75 (s, 1H), 8.53 (dd, J_{HH} = 5.2, 1.6 Hz, 1H), 8.42 (d, J_{HH} = 6.8 Hz, 1H), 8.26 (d, J_{HH} = 2.0 Hz, 1H), 8.20 (d, J_{HH} = 2.0 Hz, 1H), 8.16 (d, J_{HH} = 5.6 Hz, 1H), 7.91 ~ 7.88 (m, 2H), 7.80 (dd, J_{HH} = 5.8, 2.0 Hz, 1H), 7.35 (dd, J_{HH} = 8.2, 5.2 Hz, 1H), 7.05 (d, J_{HH} = 4.0 Hz, 1H), 6.97 (s, 1H), 4.57 (q, J_{HH} = 7.1 Hz, 2H), 4.43 (q, J_{HH} = 7.1 Hz, 2H), 2.97 (t, J_{HH} = 7.5 Hz, 2H), 1.82 ~ 1.73 (m, 2H), 1.58 (s, 9H), 1.53 ~ 1.29 (m, 12H), 0.93 ~ 0.86 (m, 3H). ^{19}F NMR (376 MHz, d_6-Acetone, 298 K): δ -60.76 (s, 3F).

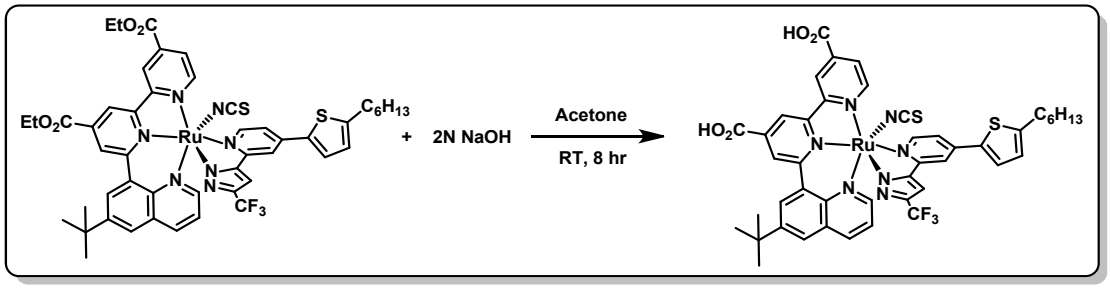

Synthesis of PRT-23

The solid of **PRT-23-E2** (81 mg, 0.08 mmol) was dissolved in a mixture of acetone (30 mL) and 2 M NaOH solution (2 mL) and stirred at room temperature overnight. Finally, the solution was concentrated, and the solid dissolved in 10 mL of H_2O and titrated with 2 N HCl to pH 3 to afford a black precipitate. This black product was washed with H_2O and acetone in sequence, yielding **PRT-23** (63 mg, 80%).

Spectral data of PRT-23: MS (FAB, ^{102}Ru): m/z 966 $(M+1)^+$. ^{1}H NMR (400 MHz, d_6-DMSO, 298 K): δ 9.08 (s, 1H), 9.01 (d, J_{HH} = 6Hz, 1H), 8.99 (s, 1H), 8.69 (s, 1H), 8.61 (s, 1H), 8.43 (d, J_{HH} = 8 Hz, 1H), 8.27 (s, 1H), 8.26 (s, 1H), 8.15 (s, 1H), 7.94 ~ 7.90 (m, 3H), 7.74 (d, J_{HH} = 6 Hz, 1H), 7.37 ~ 7.34 (m, 1H), 7.04 (s, 2H), 2.88(t, J_{HH} = 8 Hz, 2H), 1.65(m, 2H), 1.53 (s, 9H), 1.34 ~ 1.28 (m, 6H), 0.86(t, J_{HH} = 8 Hz, 3H). ^{19}F NMR (376 MHz, d_6-DMSO, 298 K): δ -56.01 (s, 3F). Anal. Calcd for $C_{45}H_{40}F_3N_7O_4RuS_2 \cdot 2H_2O$: C, 53.99; N, 9.79; H, 4.43. Found: C, 54.23; N, 9.92; H, 4.21.

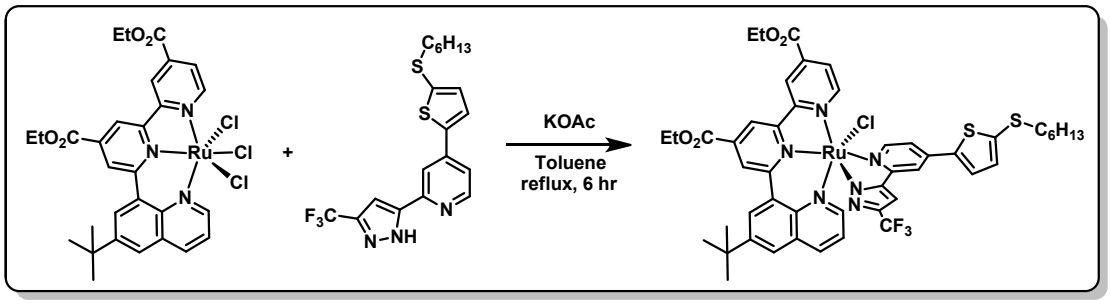

Synthesis of PRT-24-E1

A mixture of (Et-Qbpy)$RuCl_3$ (100 mg, 0.14 mmol), 4-(5-(hexylthio)thiophen-2-yl)-2-(3-(trifluoromethyl)-1H-pyrazol-5-yl)pyridine[1] (60 mg, 0.15 mmol), and KOAc (30 mg, 0.3 mmol) in 30 mL of toluene was heated to reflux for 6 h. After evaporating the solvent, the residue was purified by silica gel column chromatography (CH_2Cl_2/ethyl acetate = 8:1), yielding **PRT-24-E1** (116 mg, 78%).

Spectral data: ^{1}H NMR (400 MHz, $CDCl_3$, 298 K): δ 9.84 (d, J_{HH} = 6.4 Hz, 1H), 8.79 (s, 1H), 8.71 (s, 1H), 8.55 (s, 2H), 8.47 (s, 1H), 7.95 (d, J_{HH} = 8.0 Hz, 1H), 7.92 (d, J_{HH} = 6.0 Hz, 1H), 7.76 (s, 1H), 7.71 (s, 1H), 7.61 (d, J_{HH} = 5.6 Hz, 1H), 7.55 (d, J_{HH} = 3.6 Hz, 2H), 7.16 (d, J_{HH} = 3.6 Hz, 1H), 7.02 (dd, J_{HH} = 8.0, 5.2 Hz, 1H), 6.57 (s, 1H), 4.56 (q, J_{HH} = 7.2 Hz, 2H), 4.43 (q, J_{HH} = 7.2 Hz, 2H), 2.93 (t, J_{HH} = 7.3 Hz, 2H), 1.73 ~ 1.65 (m, 2H), 1.50 (s, 9H), 1.42 ~ 1.24 (m, 12H), 0.91 ~ 0.86 (m, 3H). ^{19}F NMR (376 MHz, $CDCl_3$, 298 K): δ -60.66 (s, 3F).

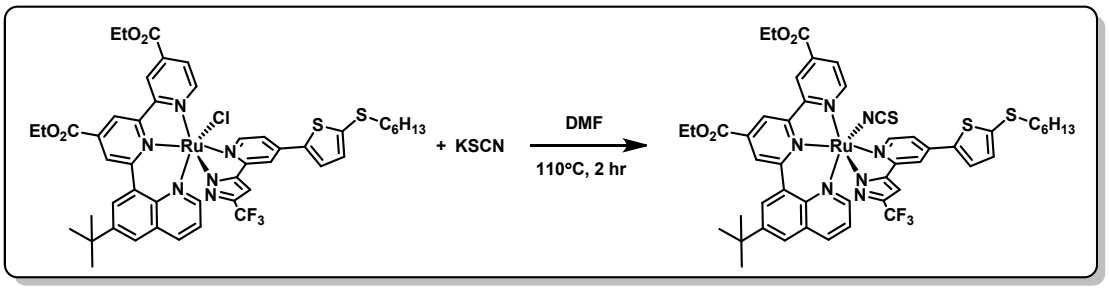

Synthesis of PRT-24-E2

A mixture of **PRT-24-E1** (116 mg, 0.11 mmol) and KSCN (102 mg, 1.1 mmol) in 30 mL of DMF was heated to reflux for 2 h. After evaporating the solvent, the residue was purified by silica gel column chromatography (CH_2Cl_2/ethyl acetate = 10:1), yielding **PRT-24-E2** (77 mg, 65%)

Spectral data: ^{1}H NMR (400 MHz, $CDCl_3$, 298 K): δ 9.28 (d, J_{HH} = 6.0 Hz, 1H), 8.77 (s, 1H), 8.69 (s, 1H), 8.57 (s, 1H), 8.48 (s, 1H), 8.31 (d, J_{HH} = 4.8 Hz, 1H), 8.03 (d, J_{HH} = 8.0 Hz, 1H), 7.85 (d, J_{HH} = 6.0 Hz, 1H), 7.82 (s, 1H), 7.72 (s, 1H), 7.63 (d, J_{HH} = 6.0 Hz, 1H), 7.58 (dd, J_{HH} = 5.8, 1.2 Hz, 1H), 7.55 (d, J_{HH} = 3.6 Hz, 1H), 7.16 (d, J_{HH} = 3.6 Hz, 1H), 7.04 (dd, J_{HH} = 8.0, 5.2 Hz, 1H), 6.60 (s, 1H), 4.59 (q, J_{HH} = 7.2 Hz, 2H), 4.45 (q, J_{HH} = 7.2 Hz, 2H), 2.94 (t, J_{HH} = 7.6 Hz, 2H), 1.73 ~ 1.66 (m, 2H), 1.51 (s, 9H), 1.46 ~ 1.22 (m, 12H), 0.91 ~ 0.86 (m, 3H). ^{19}F NMR (376 MHz, $CDCl_3$, 298 K): δ -60.66 (s, 3F).

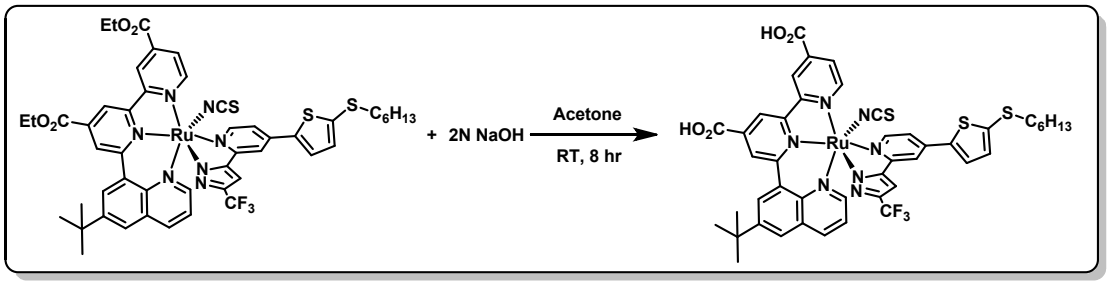

Synthesis of PRT-24

The solid of **PRT-24-E2** (81 mg, 0.08 mmol) was dissolved in a mixture of acetone (30 mL) and 2 M NaOH solution (2 mL) and stirred at room temperature overnight. Finally, the solution was concentrated, and the solid dissolved in 10 mL of H_2O and titrated with 2 N HCl to pH 3 to afford a black precipitate. This black product was washed with H_2O and acetone in sequence, yielding **PRT-24** (64 mg, 83%).

Spectral dataof PRT-24: MS (FAB, ^{102}Ru): m/z 998 $(M+1)^+$. ^{1}H NMR (400 MHz, d_6-DMSO, 298 K): δ 9.12 (s, 1H), 9.06 (d, J_{HH} = 6 Hz, 1H), 9.03 (s, 1H), 8.72 (s, 1H), 8.65 (s, 1H), 8.47 (d, J_{HH} = 8 Hz, 1H), 8.34 (s, 1H), 8.28 (d, J_{HH} = 6 Hz, 1H), 8.18 (s, 1H), 8.04 ~ 7.99 (m, 2H), 7.93 (d, J_{HH} = 6 Hz, 1H), 7.76 (d, J_{HH} = 6 Hz, 1H), 7.40 ~ 7.35 (m, 2H), 7.04 (s, 1H), 2.99 (t, J_{HH} = 8 Hz, 2H), 1.63 (m, 2H), 1.47 (s, 9H), 1.43 ~ 1.25 (m, 6H), 0.87 (t, J_{HH} = 8 Hz, 3H). ^{19}F NMR (376 MHz, d_6-DMSO, 298 K): δ -58.86 (s, 3F). Anal. Calcd for $C_{45}H_{40}F_3N_7O_4RuS_3 \cdot 2H_2O$: C, 52.31; N, 9.49; H, 4.29. Found: C, 52.11; N, 9.81; H, 4.66.

TD-DFT Calculation

All calculations were performed by Gaussian 09 program. Their ground state

structures were first optimized with density functional theory (DFT) at B3LYP/LANL2DZ (Ru) and 6-31G* (H, C, N, O, F, S) level. The optimized structures were then used to calculate 60 lowest singlet energy optical excitations using the time-dependent density functional theory (TD-DFT) method. Their lowest ground triplet state energies were also calculated. A polarizable continuum model (PCM) in Gaussian 09 was applied using dimethylformamide (DMF) as the solvent.

Photovoltaic Characterization.

Photovoltaic measurements were tested under a class-AAA solar simulator (Model 11016A, Sun 3000, ABET Technologies) equipped with a 550 W xenon light source and water-cooling stage (25 °C). The output power density was calibrated to be 100 mW/cm^2 using a certificated KG-5 Si reference cell and with a circular aperture of 8 mm. The current-voltage characteristic of each cell was obtained with adopting 4-wire sense mode, delay time set as 100 ms and bias scan from short-circuit to open-circuit by using a Keithley digital source meter (Model 2400). The spectra of incident photon-to-current conversion efficiency (IPCE) were calculated with the equation of $1240 \cdot J_{SC}(\lambda)/(\lambda \cdot P_{in}(\lambda))$ where J_{SC} is the short-circuit current density under each monochromatic illumination in unit of A/cm^2, λ is the wavelength of incident monochromatic light in unit of nanometer, and P_{in} is the monochromatic light intensity in unit of W/cm^2 and were plotted as a function of incident wavelength with an increment of 10 nm. The current was pre-amplified by a current amplifier (SR570) and measured by Keithley 2400. It should be noted that 10 values of J_{SC} (interval 50 ms) were collected sequentially after illuminating the device for 3 seconds and then averaged for calculation of IPCE. A 300 W Xe lamp (Model 6258, Newport Oriel) combined with an Oriel cornerstone 260 1/4 m monochromator (Model 74100) provided a device under test with a monochromatic beam (dc mode). The beam power intensity was calibrated with a power meter (Model 1936-C, Newport) equipped with a Newport 818-UV photodetector.

Transient Absorption Spectroscopy, Charge Extraction and Transient Photovoltage Measurements

Transient absorption spectroscopy (TAS) measurements were carried out on 1 cm^2 DSC devices on a system similar to that used by Durrent and co-workers.[4] Charge extraction (CE) and transient photovoltage (TPV) measurements were carried out on optimized 0.16 cm^2 DSC devices using a system similar to that empolyed by O'Regan *et al.*[5]

Electrical Impedance Measurements

Electrical impedance experiments were carried out with a PARSTAT 2273 (AMETEK Princeton Applied Research, U.S.A.) electrochemical workstation in dark under forward bias, with a frequency range of 0.1 – 100 kHz and a potential modulation of 10 mV.

Charge extraction and intensity-modulated photovoltage spectroscopy

Charge extraction (CE) was measured with the PGSTAT302N electrochemical workstation (Autolab) at an open-circuit condition for the photovoltage of the device to attain a steady state. The red light-emitting diode (LED, 627 nm) was switched off while the device was simultaneously switched to a short-circuit condition to measure the excess charges generated in the film.[6, 7] Intensity-modulated photovoltage spectroscopy (IMVS) measurement was conducted using the same electrochemical workstation equipped with a frequency response analyzer (FRA) to drive a red light emitting diode. The analysis of the photovoltage response of the cells was conducted in the frequency range of 10^4 – 1 Hz and LED supplied the AC (modulation depth 10%) perturbation current superimposed on the DC current.

Table S1. The wavelengths, transition probabilities and charge transfer characters of the singlet optical transitions in selected states with oscillator strength > 0.03 over 300 nm for **PRT-21** in DMF.

State	λ_{cal} (nm)	*f*	Assignments	MLCT
T_1	812.8	0	HOMO→LUMO(95%)	34.66%
S_1	738	0.0317	HOMO→LUMO(96%)	35.02%
S_2	613.7	0.0004	HOMO-2→LUMO(88%) HOMO-4→LUMO(6%)	35.22%
S_4	531	0.0693	HOMO→LUMO+1(61%) HOMO-1→LUMO(30%)	34.33%
S_5	519.6	0.0351	HOMO-1→LUMO+1(95%)	33.25%
S_7	469.6	0.1162	HOMO→LUMO+2(95%)	42.39%
S_{11}	431.2	0.0486	HOMO→LUMO+4(57%) HOMO-1→LUMO+2(39%)	39.10%
S_{16}	399.8	0.0609	HOMO-3→LUMO+1(66%) HOMO-6→LUMO(23%)	3.03%
S_{17}	398.8	0.1723	HOMO-6→LUMO(47%) HOMO-3→LUMO+1(33%) HOMO-2→LUMO+4(8%)	13.78%
S_{20}	377.7	0.1869	HOMO-4→LUMO+1(68%) HOMO-2→LUMO+4(17%) HOMO-5→LUMO+1(10%)	18.63%
S_{21}	366.6	0.1835	HOMO-5→LUMO+1(34%) HOMO-2→LUMO+4(28%) HOMO-4→LUMO+1(21%) HOMO-2→LUMO+1(6%)	26.83%
S_{24}	355.7	0.0792	HOMO-5→LUMO+1(46%) HOMO-2→LUMO+4(30%) HOMO-6→LUMO(8%)	27.56%
S_{27}	345.8	0.0485	HOMO-8→LUMO(81%)	-3.75%
S_{28}	338.4	0.0499	HOMO-3→LUMO+3(79%) HOMO-3→LUMO+4(14%)	-1.31%
S_{31}	333.4	0.1008	HOMO-3→LUMO+4(63%) HOMO-3→LUMO+3(18%) HOMO→LUMO+6(6%)	0.67%
S_{32}	331.3	0.0662	HOMO-1→LUMO+5(55%) HOMO→LUMO+6(35%)	36.75%
S_{33}	330.1	0.0533	HOMO→LUMO+6(49%) HOMO-1→LUMO+5(34%) HOMO-6→LUMO+2(7%)	37.27%
S_{34}	325.6	0.1193	HOMO-9→LUMO(46%) HOMO-5→LUMO+2(34%) HOMO-4→LUMO+2(12%)	13.70%
S_{35}	322.3	0.0328	HOMO-4→LUMO+3(69%) HOMO-6→LUMO+2(16%) HOMO-5→LUMO+3(7%)	17.47%
S_{37}	321.7	0.2555	HOMO-5→LUMO+2(47%) HOMO-9→LUMO(37%)	15.25%
S_{40}	315	0.1481	HOMO-4→LUMO+4(84%)	11.06%
S_{46}	305.8	0.1566	HOMO-5→LUMO+4(47%) HOMO-2→LUMO+6(36%)	29.93%

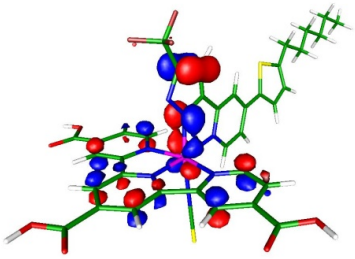	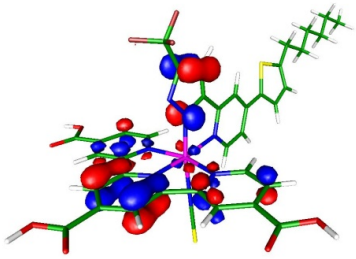	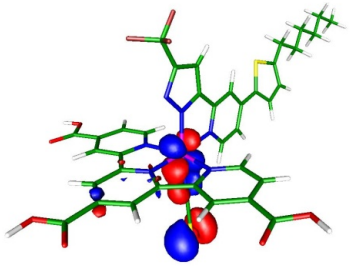
HOMO-9 (-7.35 eV)	HOMO-8 (-7.15 eV)	HOMO-6 (-6.58 eV)
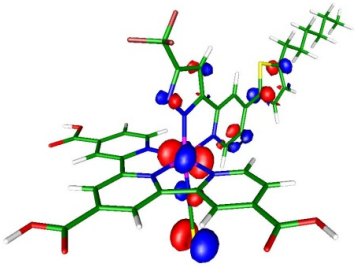	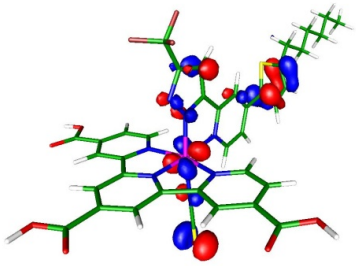	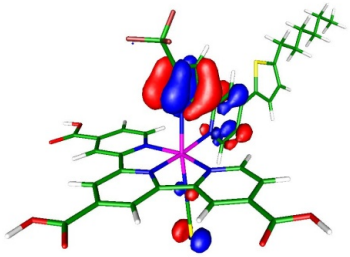
HOMO-5 (-6.49 eV)	HOMO-4 (-6.30 eV)	HOMO-3 (-6.18 eV)
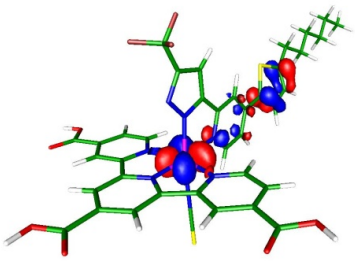	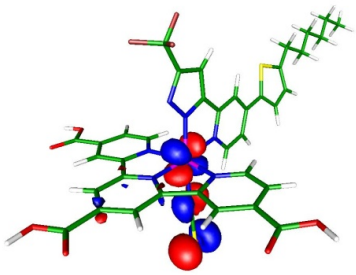	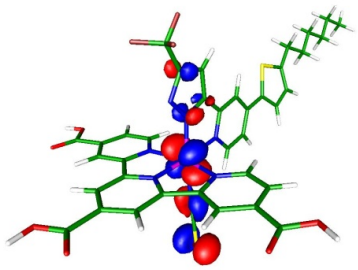
HOMO-2 (-5.79 eV)	HOMO-1 (-5.61 eV)	HOMO (-5.39 eV)
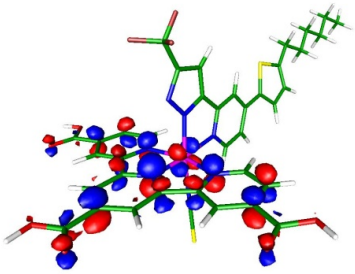	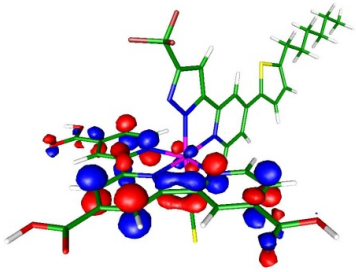	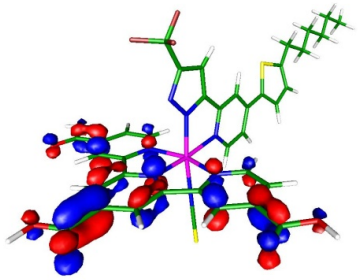
LUMO (-3.71 eV)	LUMO+1 (-2.54 eV)	LUMO+2 (-2.18 eV)

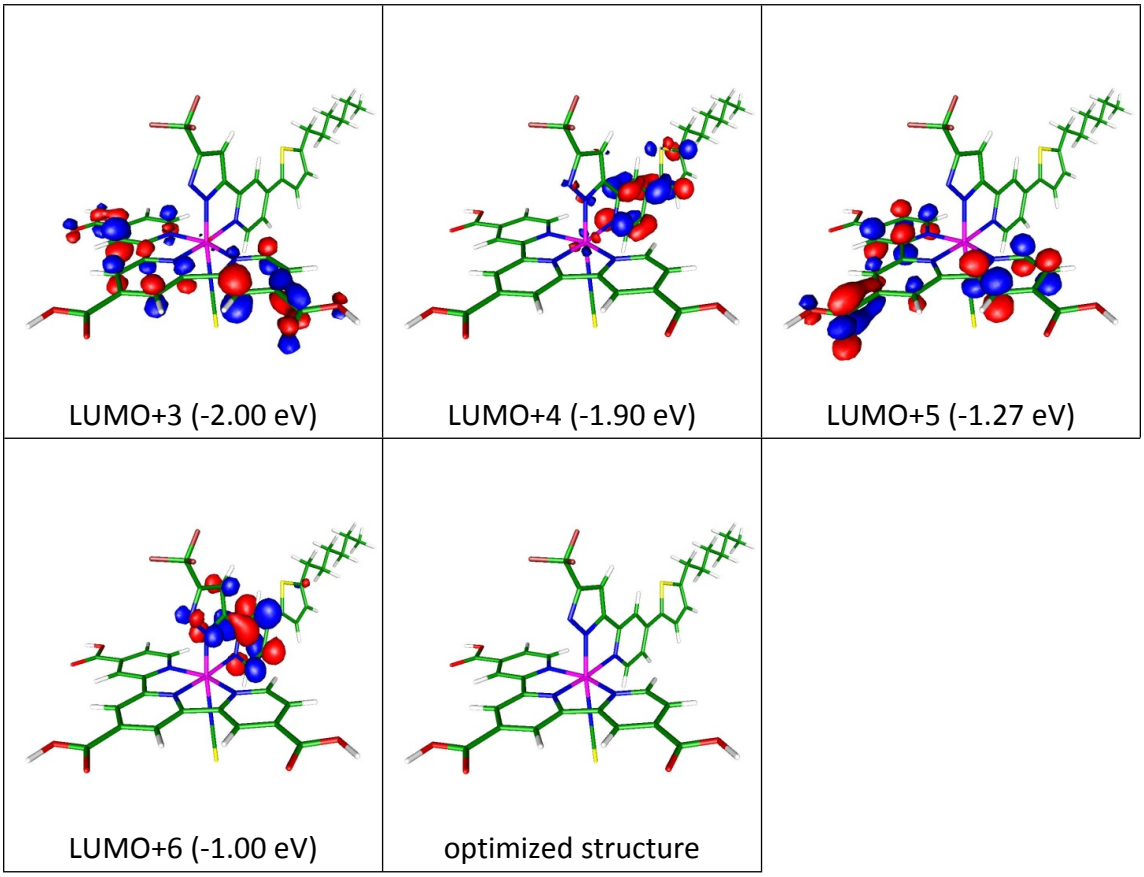

Figure S1. Frontier molecular orbitals and optimized structure pertinent to the singlet optical transitions in selected states for **PRT-21**.

Table S2. The wavelengths, transition probabilities and charge transfer characters of the singlet optical transitions in selected states with oscillator strength > 0.02 over 300 nm for **PRT-22** in DMF.

State	λ_{cal} (nm)	*f*	Assignments	MLCT
T_1	813.1	0	HOMO→LUMO(95%)	34.74%
S_1	738.2	0.0319	HOMO→LUMO(96%)	35.11%
S_2	625.8	0.0004	HOMO-1→LUMO(67%) HOMO-3→LUMO(29%)	18.29%
S_4	531.1	0.0791	HOMO→LUMO+1(61%) HOMO-2→LUMO(30%)	34.39%
S_5	519.1	0.0348	HOMO-2→LUMO+1(95%)	33.29%
S_8	469.5	0.1173	HOMO→LUMO+2(95%)	42.46%
S_{13}	428.5	0.0707	HOMO-2→LUMO+2(79%) HOMO→LUMO+4(8%) HOMO-6→LUMO(7%)	35.23%
S_{17}	403.6	0.5438	HOMO-6→LUMO(44%) HOMO-1→LUMO+3(28%) HOMO-1→LUMO+4(16%)	18.45%
S_{19}	400.9	0.0394	HOMO-1→LUMO+3(50%) HOMO-1→LUMO+4(17%) HOMO-6→LUMO(11%) HOMO-3→LUMO+3(11%)	19.74%
S_{21}	383	0.4134	HOMO-1→LUMO+4(43%) HOMO-5→LUMO+1(30%) HOMO-6→LUMO(14%)	15.96%
S_{23}	364.1	0.0415	HOMO-5→LUMO+1(62%) HOMO-1→LUMO+4(13%) HOMO-6→LUMO(11%)	16.10%
S_{28}	347.5	0.0311	HOMO-3→LUMO+3(77%) HOMO-1→LUMO+3(11%) HOMO-3→LUMO+4(5%)	40.35%
S_{29}	346.6	0.0435	HOMO-7→LUMO(81%)	-3.61%
S_{30}	343.7	0.0609	HOMO-3→LUMO+4(66%) HOMO→LUMO+6(7%) HOMO-4→LUMO+3(7%) HOMO-3→LUMO+3(5%)	35.44%
S_{31}	337.2	0.0252	HOMO-4→LUMO+3(80%) HOMO→LUMO+6(8%)	5.06%
S_{33}	333.4	0.0687	HOMO-4→LUMO+4(50%) HOMO→LUMO+6(24%) HOMO-1→LUMO+6(10%) HOMO-4→LUMO+3(10%)	12.92%
S_{37}	324.2	0.0873	HOMO-1→LUMO+5(63%) HOMO-9→LUMO(17%) HOMO-3→LUMO+5(12%)	17.91%
S_{38}	323	0.3129	HOMO-9→LUMO(55%) HOMO-1→LUMO+5(19%) HOMO-5→LUMO+2(13%)	7.80%
S_{41}	313.1	0.0222	HOMO-5→LUMO+4(46%) HOMO-1→LUMO+6(32%)	14.88%
S_{47}	305.5	0.0734	HOMO-5→LUMO+4(44%) HOMO-1→LUMO+6(44%)	16.73%

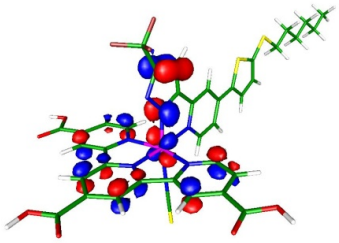 HOMO-9 (-7.33 eV)	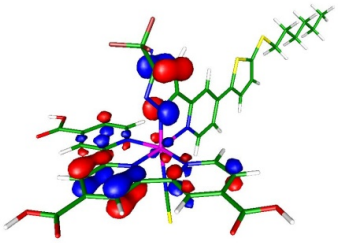 HOMO-7 (-7.14 eV)	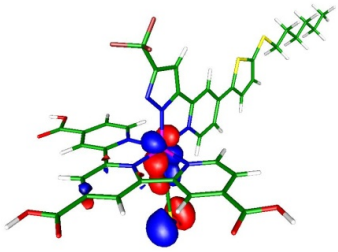 HOMO-6 (-6.58 eV)
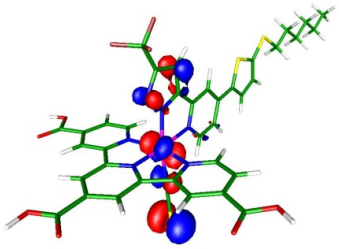 HOMO-5 (-6.44 eV)	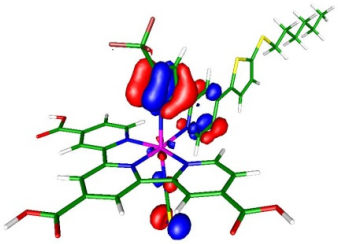 HOMO-4 (-6.19 eV)	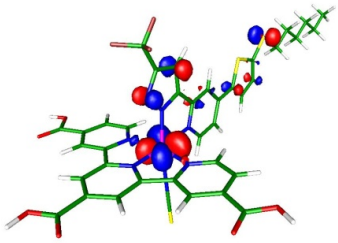 HOMO-3 (-6.09 eV)
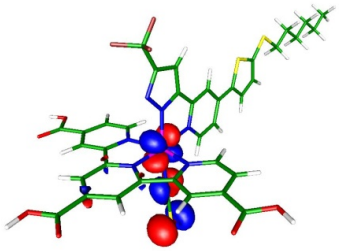 HOMO-2 (-5.61 eV)	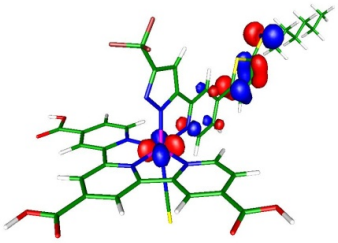 HOMO-1 (-5.57 eV)	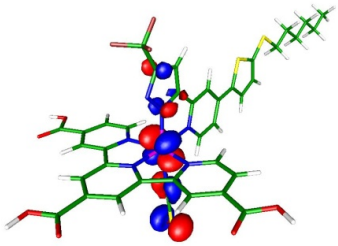 HOMO (-5.39 eV)
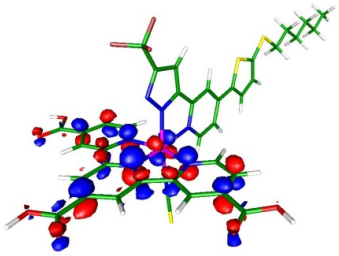 LUMO (-3.71 eV)	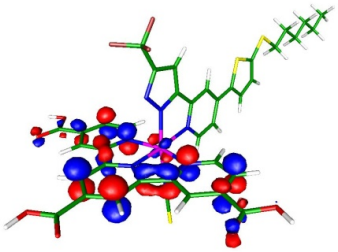 LUMO+1 (-2.54 eV)	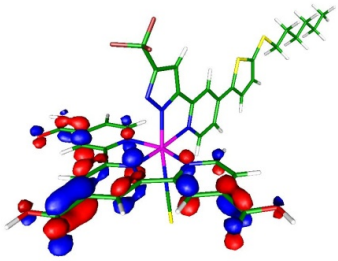 LUMO+2 (-2.18 eV)

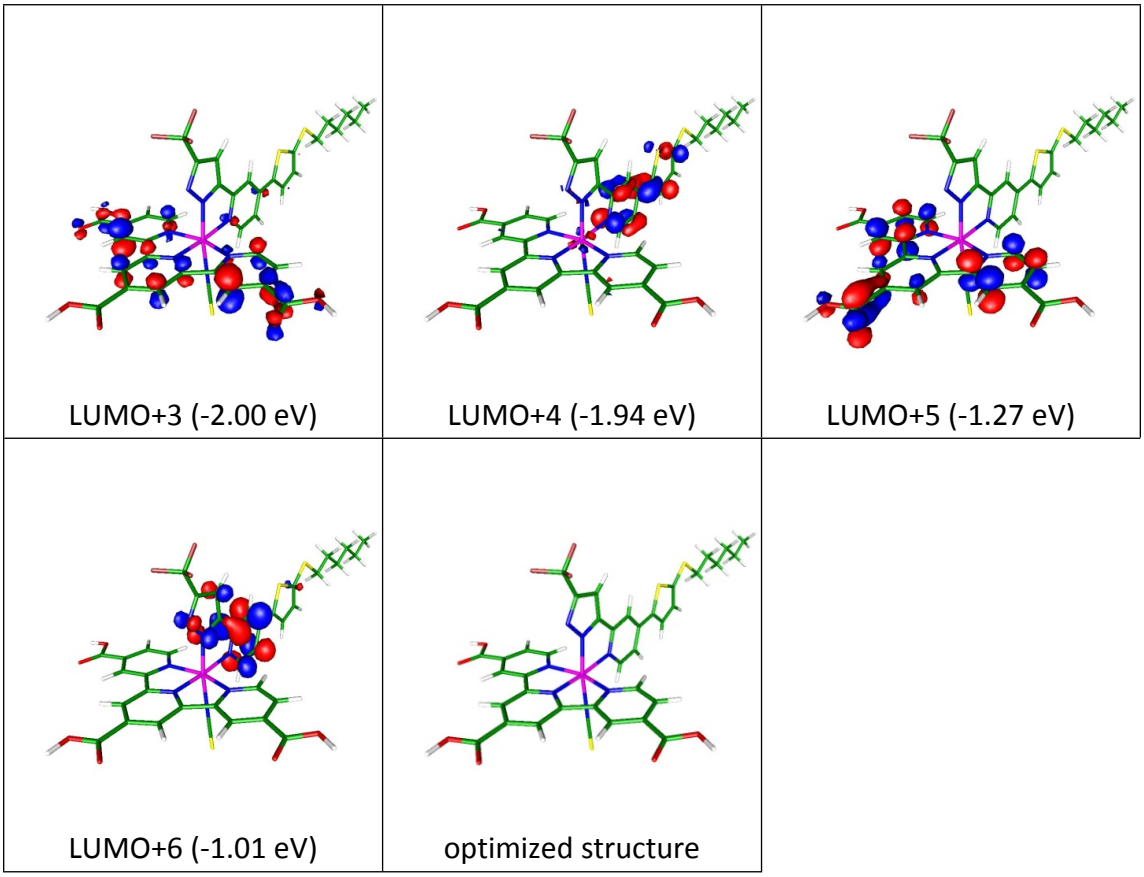

Figure S2. Frontier molecular orbitals and optimized structure pertinent to the singlet optical transitions in selected states for **PRT-22**.

Table S3. The wavelengths, transition probabilities and charge transfer characters of the singlet optical transitions in selected states with oscillator strength > 0.02 over 300 nm for **PRT-23** in DMF. The lowest triplet optical transition ($S_0 \rightarrow T_1$) is also listed.

State	λ_{cal} (nm)	f	Assignments	MLCT
T_1	784.8	0	HOMO→LUMO(92%)	39.95%
S_1	701.8	0.0241	HOMO→LUMO(93%)	40.38%
S_2	579.7	0.0476	HOMO-1→LUMO(70%) HOMO→LUMO+1(21%)	37.53%
S_4	521.9	0.0409	HOMO→LUMO+1(68%) HOMO-1→LUMO(16%)	39.45%
S_6	479.5	0.1127	HOMO→LUMO+2(90%)	45.57%
S_{16}	391.8	0.2118	HOMO-6→LUMO(43%) HOMO-1→LUMO+4(31%) HOMO-2→LUMO+3(14%)	31.06%
S_{17}	386.5	0.054	HOMO-5→LUMO(65%) HOMO-2→LUMO+3(10%) HOMO-4→LUMO(9%) HOMO-2→LUMO(5%)	17.21%
S_{19}	373	0.1661	HOMO-2→LUMO+3(53%) HOMO-2→LUMO+4(14%) HOMO-5→LUMO(6%)	36.64%
S_{20}	365.5	0.1863	HOMO-7→LUMO(83%) HOMO-4→LUMO+1(5%)	0.08%
S_{24}	348.9	0.1418	HOMO→LUMO+5(56%) HOMO-6→LUMO+1(20%)	34.22%
S_{26}	346.6	0.05	HOMO-6→LUMO+1(39%) HOMO-5→LUMO+1(21%) HOMO→LUMO+5(15%)	22.93%
S_{28}	339.6	0.1297	HOMO-3→LUMO+3(80%) HOMO-2→LUMO+5(6%)	1.74%
S_{29}	336.5	0.0445	HOMO-4→LUMO+2(80%) HOMO-5→LUMO+2(7%)	7.74%
S_{35}	322	0.0683	HOMO-4→LUMO+3(33%) HOMO-2→LUMO+10(24%) HOMO-2→LUMO+9(9%)	7.94%
S_{38}	317.3	0.082	HOMO-9→LUMO(28%) HOMO-7→LUMO+1(26%) HOMO-1→LUMO+6(16%) HOMO→LUMO+7(7%)	11.52%
S_{39}	316.3	0.0959	HOMO-10→LUMO(42%) HOMO-7→LUMO+1(22%) HOMO-9→LUMO(14%) HOMO→LUMO+7(8%)	4.35%
S_{40}	315.3	0.0538	HOMO→LUMO+7(35%) HOMO-1→LUMO+6(10%) HOMO-6→LUMO+2(9%) HOMO-7→LUMO+1(8%) HOMO-5→LUMO+2(5%)	26.06%
S_{41}	313.1	0.0509	HOMO-3→LUMO+4(48%) HOMO-1→LUMO+6(22%)	9.39%
S_{43}	311	0.2123	HOMO-2→LUMO+5(35%) HOMO-5→LUMO+3(33%)	28.57%
S_{49}	300.8	0.0538	HOMO-2→LUMO+5(40%) HOMO-5→LUMO+3(34%) HOMO-11→LUMO(5%)	28.55%

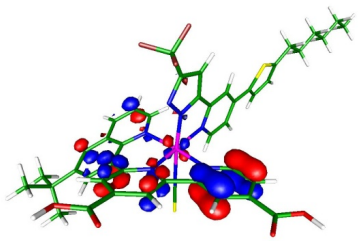 HOMO-11 (-7.49 eV)	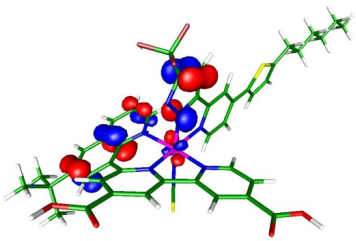 HOMO-10 (-7.16 eV)	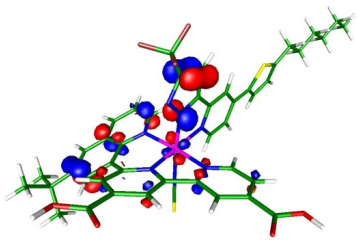 HOMO-9 (-7.15 eV)
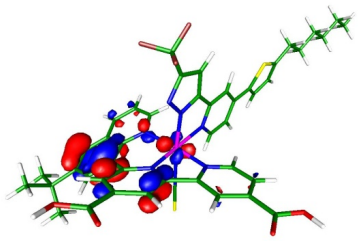 HOMO-7 (-6.66 eV)	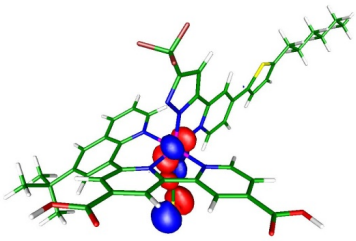 HOMO-6 (-6.46 eV)	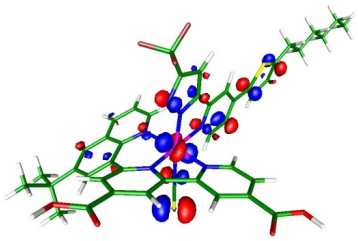 HOMO-5 (-6.43 eV)
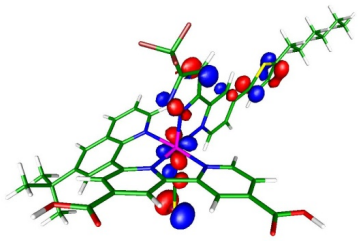 HOMO-4 (-6.23 eV)	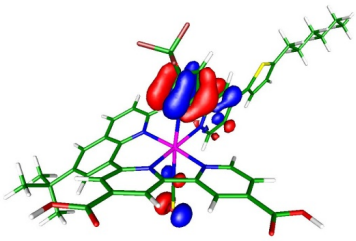 HOMO-3 (-6.13 eV)	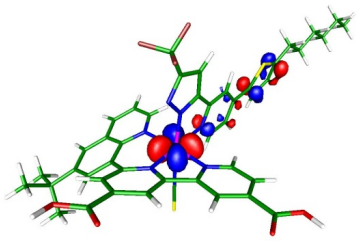 HOMO-2 (-5.77 eV)
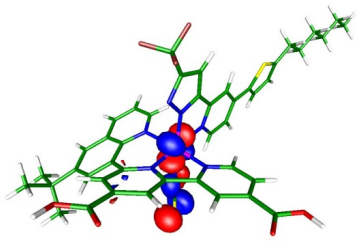 HOMO-1 (-5.48 eV)	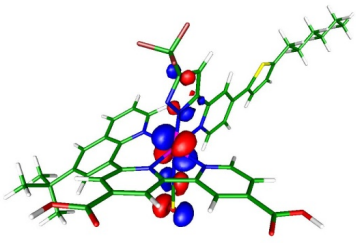 HOMO (-5.25 eV)	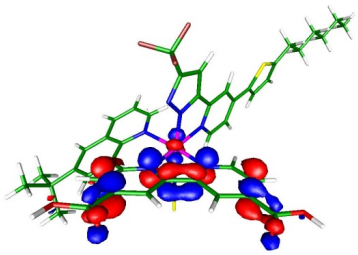 LUMO (-3.48 eV)

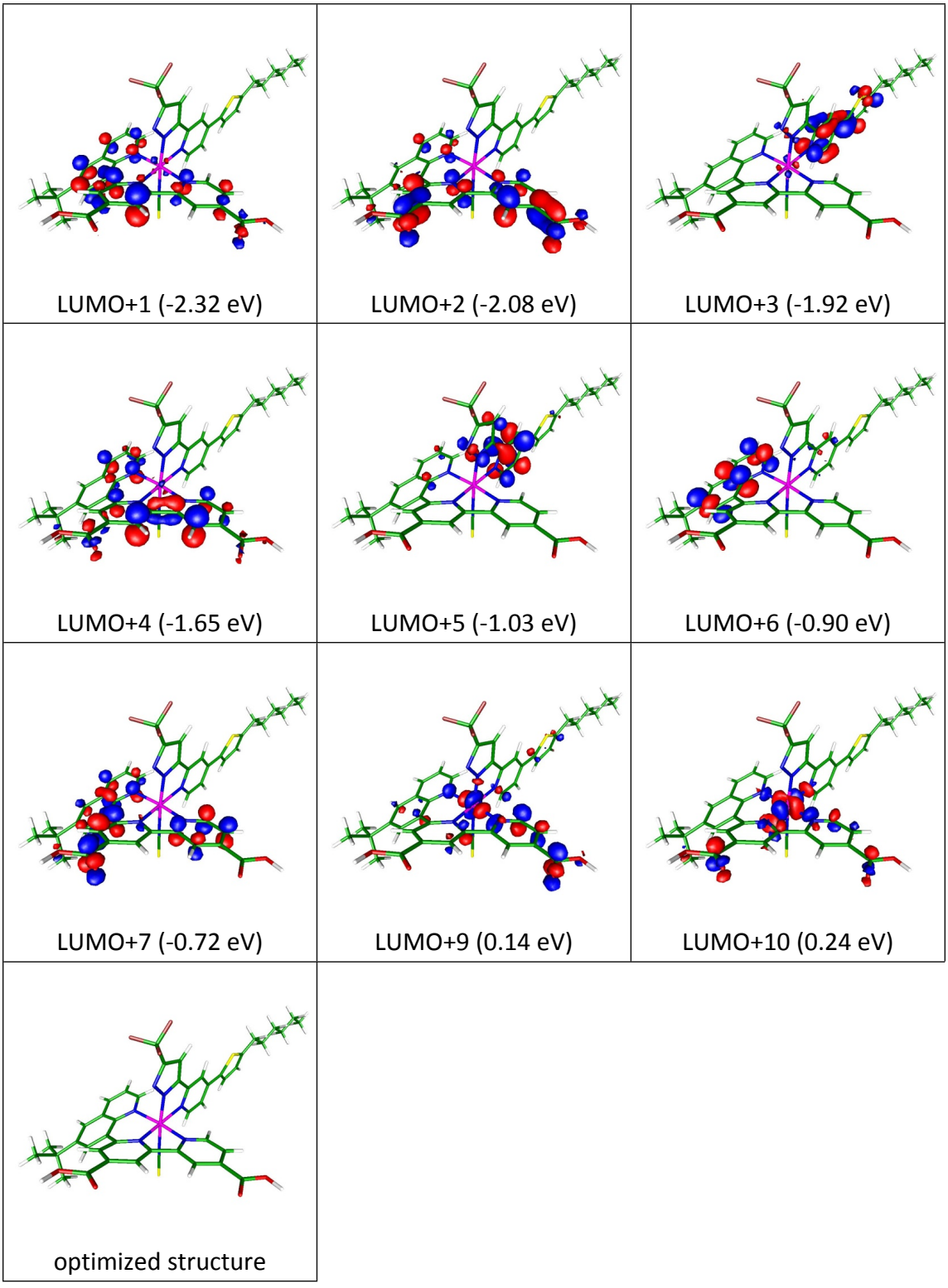

Figure S3. Frontier molecular orbitals and optimized structure pertinent to the singlet optical transitions in selected states for **PRT-23**.

Table S4. The wavelengths, transition probabilities and charge transfer characters of the singlet optical transitions in selected states with oscillator strength > 0.02 over 300 nm for **PRT-24** in DMF.

State	λ_{cal} (nm)	*f*	Assignments	MLCT
T_1	785.4	0	HOMO→LUMO(92%)	39.80%
S_1	703	0.0238	HOMO→LUMO(93%)	40.23%
S_2	579.7	0.0499	HOMO-1→LUMO(67%) HOMO→LUMO+1(21%)	35.73%
S_4	522.3	0.0526	HOMO→LUMO+1(69%) HOMO-1→LUMO(18%)	40.47%
S_5	495.3	0.0488	HOMO-1→LUMO+1(90%)	39.17%
S_6	480.1	0.117	HOMO→LUMO+2(88%)	44.44%
S_{10}	443.6	0.046	HOMO-1→LUMO+2(93%)	42.13%
S_{16}	398	0.4996	HOMO-6→LUMO(45%) HOMO-2→LUMO+3(39%) HOMO-1→LUMO+4(7%)	19.54%
S_{17}	395.7	0.2091	HOMO-1→LUMO+4(79%) HOMO-2→LUMO+3(14%)	37.54%
S_{19}	380.6	0.1576	HOMO-6→LUMO(32%) HOMO-2→LUMO+3(27%) HOMO-1→LUMO+4(8%) HOMO-2→LUMO+4(6%)	16.36%
S_{21}	367	0.0512	HOMO-2→LUMO+4(53%) HOMO-7→LUMO(17%) HOMO-3→LUMO+4(12%)	15.82%
S_{22}	366	0.1659	HOMO-7→LUMO(70%) HOMO-2→LUMO+4(8%) HOMO-5→LUMO+1(6%)	2.15%
S_{24}	356	0.1887	HOMO-3→LUMO+3(52%) HOMO→LUMO+5(20%) HOMO-5→LUMO+1(15%)	32.88%
S_{27}	347.8	0.0364	HOMO-6→LUMO+1(67%) HOMO→LUMO+5(17%) HOMO-3→LUMO+3(6%)	26.77%
S_{29}	345	0.0405	HOMO→LUMO+5(32%) HOMO-4→LUMO+2(24%) HOMO-3→LUMO+3(20%) HOMO-6→LUMO+1(10%)	27.22%
S_{30}	335.2	0.0544	HOMO-4→LUMO+3(60%) HOMO-1→LUMO+5(11%) HOMO-2→LUMO+5(9%)	8.54%
S_{32}	331.4	0.0363	HOMO-5→LUMO+2(85%)	18.67%
S_{40}	317.3	0.05	HOMO-9→LUMO(28%) HOMO-7→LUMO+1(21%) HOMO-1→LUMO+6(19%) HOMO→LUMO+7(13%)	13.72%
S_{41}	316.6	0.1073	HOMO-9→LUMO(44%) HOMO-7→LUMO+1(27%) HOMO-8→LUMO(11%)	-1.86%
S_{46}	308.4	0.0366	HOMO-2→LUMO+5(44%) HOMO-5→LUMO+3(22%) HOMO-4→LUMO+4(14%)	15.13%

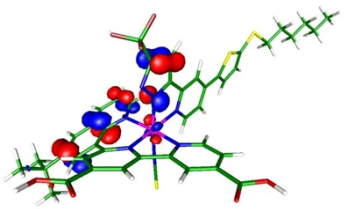 HOMO-9 (-7.15 eV)	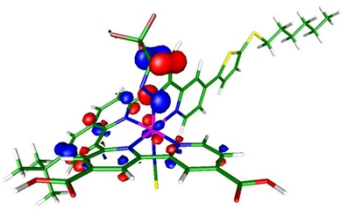 HOMO-8 (-7.14 eV)	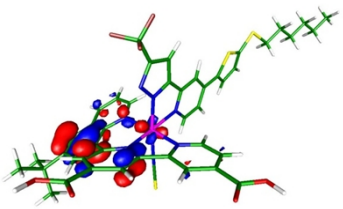 HOMO-7 (-6.66 eV)
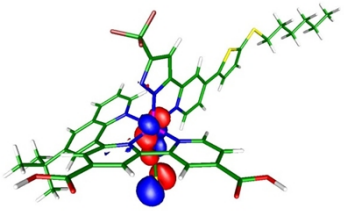 HOMO-6 (-6.45 eV)	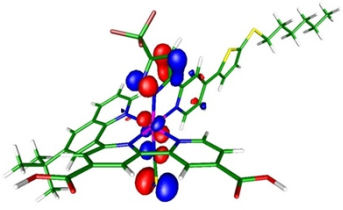 HOMO-5 (-6.35 eV)	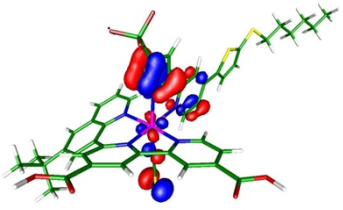 HOMO-4 (-6.17 eV)
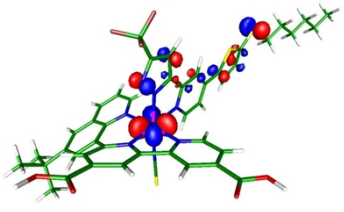 HOMO-3 (-6.00 eV)	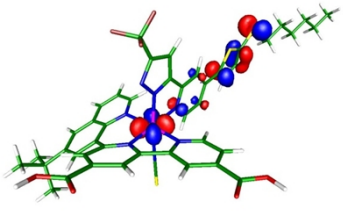 HOMO-2 (-5.59 eV)	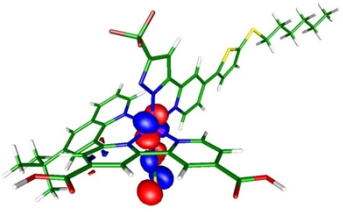 HOMO-1 (-5.47 eV)
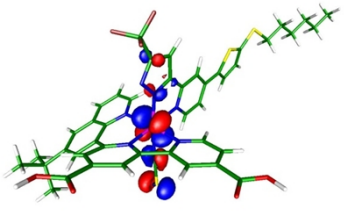 HOMO (-5.25 eV)	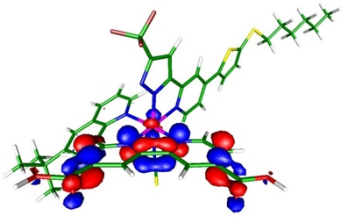 LUMO (-3.49 eV)	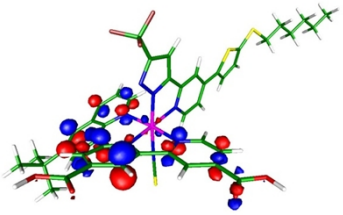 LUMO+1 (-2.32 eV)
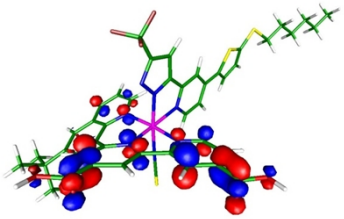 LUMO+2 (-2.08 eV)	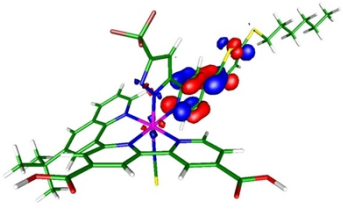 LUMO+3 (-1.95 eV)	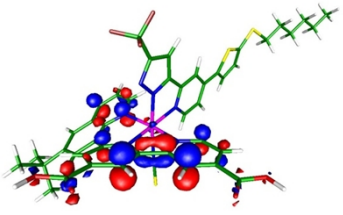 LUMO+4 (-1.65 eV)

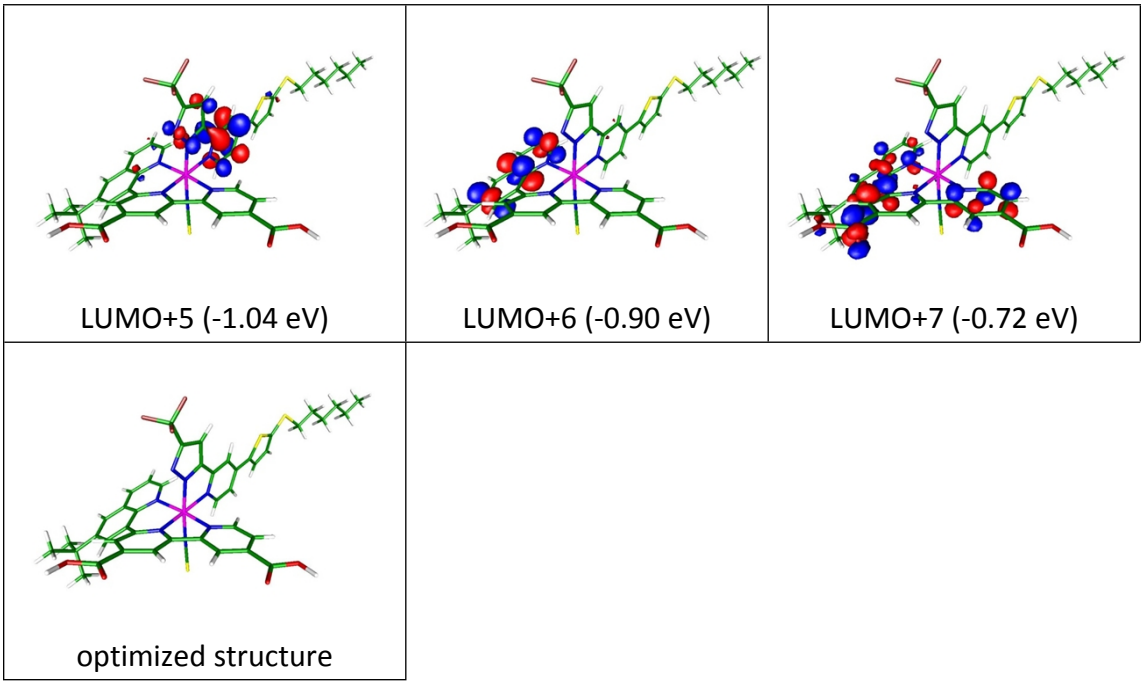

Figure S4. Frontier molecular orbitals and optimized structure pertinent to the singlet optical transitions in selected states for **PRT-24**.

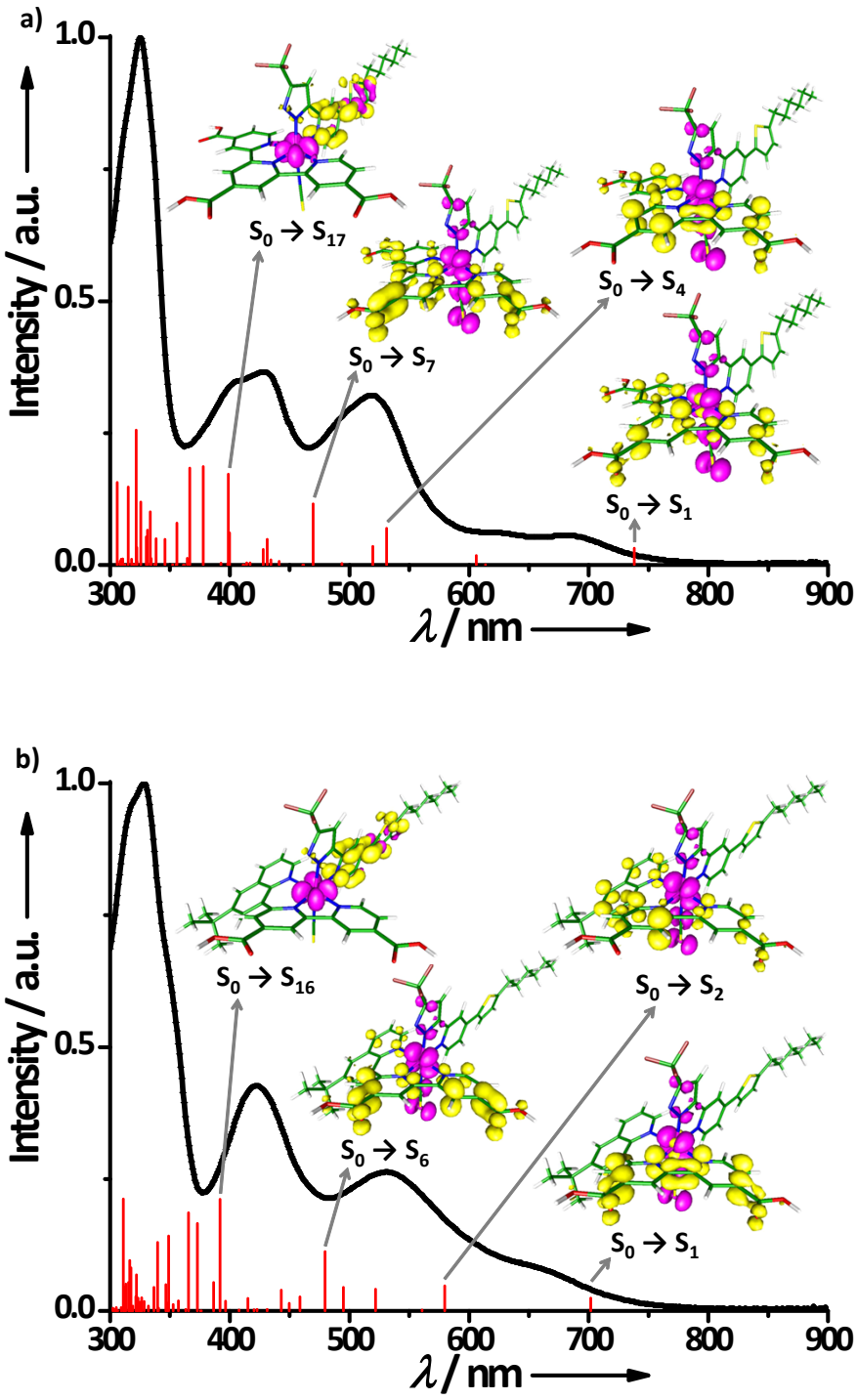

Figure S5. UV/Vis spectra and spin density plots for the specified transition of (a) **PRT-21** (top) and (b) **PRT-23** (bottom). Also depicted are the TD-DFT calculated absorption wavelengths (vertical lines) and the relative transition probability (magnitude of vertical lines). Selected frontier orbitals (pink: occupied orbital, yellow: unoccupied orbital) that contribute to the major transitions are also shown.

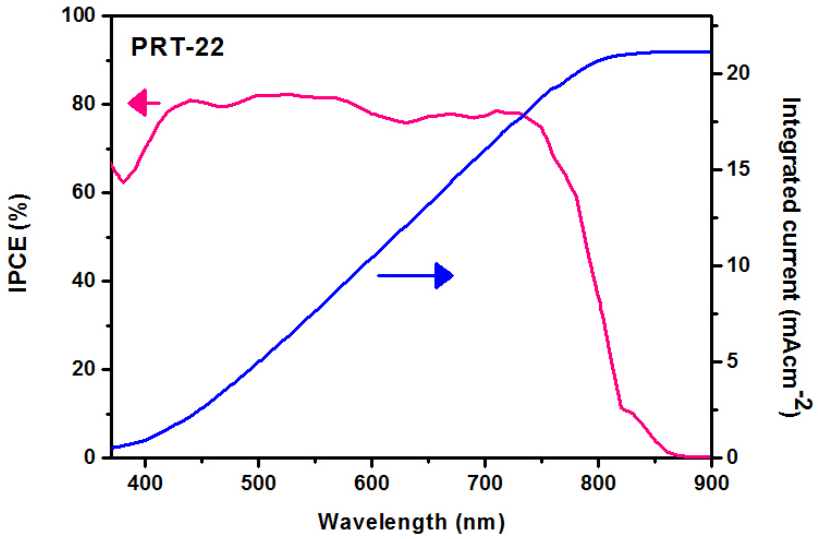

Figure S6. IPCE spectra of **PRT-22** sensitized device. The right axis indicates the integrated photocurrent that is expected to be generated under AM1.5G irradiation.

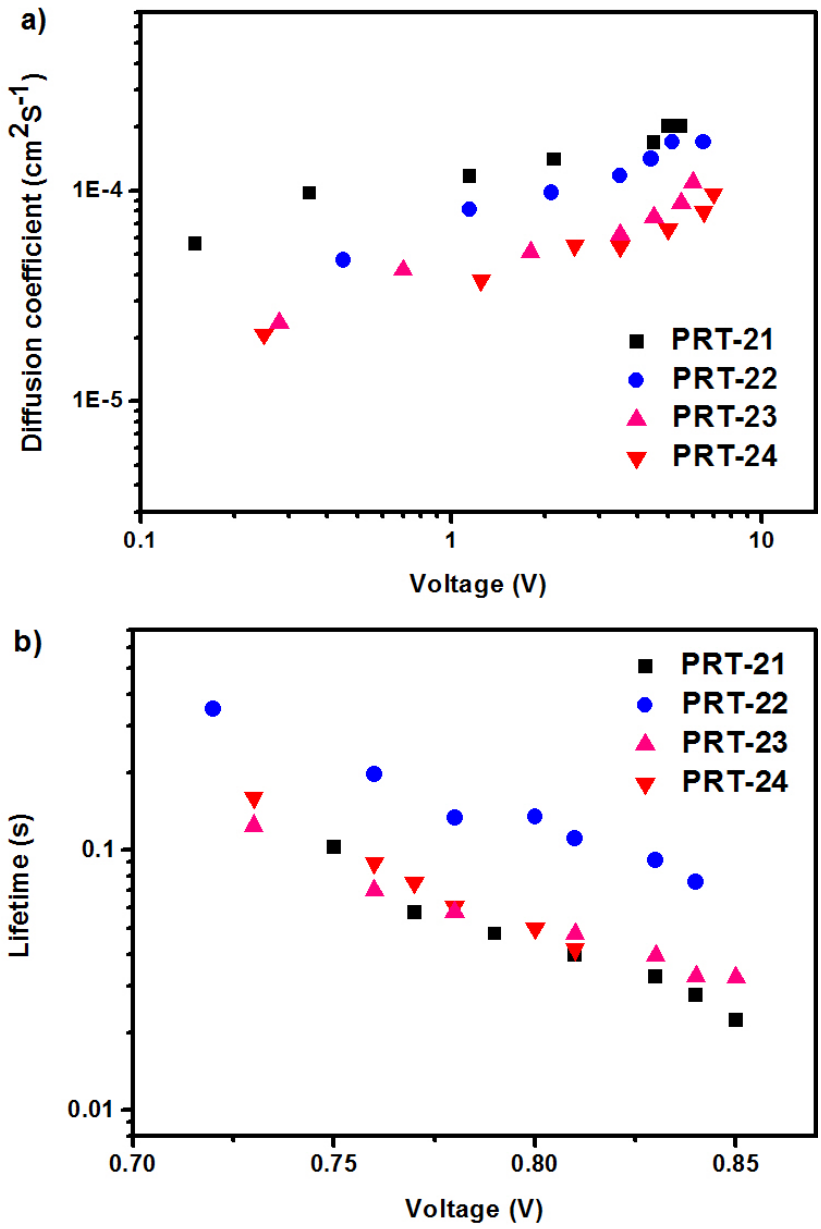

Figure S7. (a) Electron diffusion coefficient (*D*) versus *J*sc obtained from IMPS measurement and (b) electron lifetime versus voltage obtained by IMVS measurement.

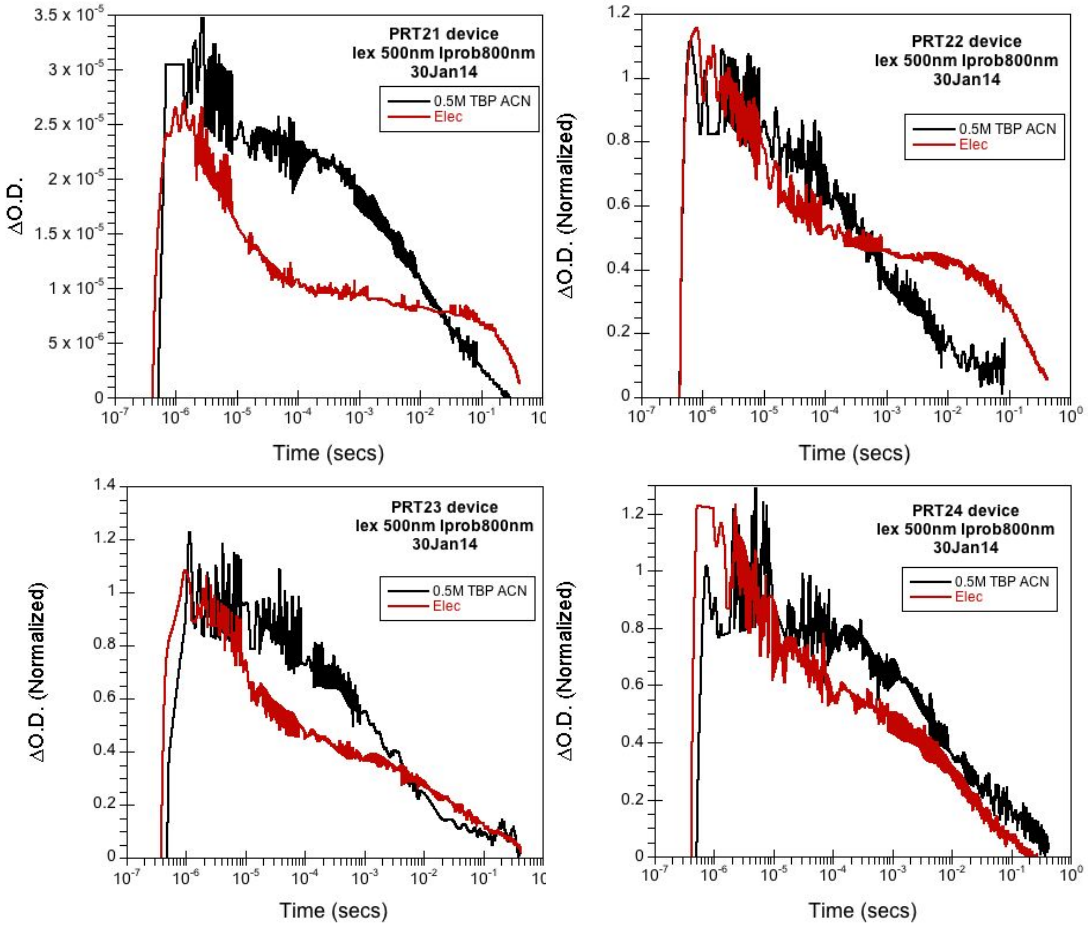

Figure S8. Transient absorption kinetics of DSC devices containing 10 μm TiO_2 films sensitized with **PRT 21 ~ 24** dyes. Kinetics were recorded at 800 nm following excitation at 500 nm.

References:

1. S.-W. Wang, K.-L. Wu, E. Ghadiri, M. G. Lobello, S.-T. Ho, Y. Chi, J.-E. Moser, F. De Angelis, M. Grätzel and M. K. Nazeeruddin, *Chem. Sci.*, 2013, **4**, 2423.
2. M. K. Nazeeruddin, P. Péchy, T. Renouard, S. M. Zakeeruddin, R. Humphry-Baker, P. Comte, P. Liska, L. Cevey, E. Costa, V. Shklover, L. Spiccia, G. B. Deacon, C. A. Bignozzi and M. Grätzel, *J. Am. Chem. Soc.*, 2001, **123**, 1613.
3. K.-L. Wu, H.-C. Hsu, K. Chen, Y. Chi, M.-W. Chung, W.-H. Liu and P.-T. Chou, *Chem. Commun.*, 2010, **46**, 5124.
4. J. N. Clifford, E. Palomares, M. K. Nazeeruddin, M. Grätzel, J. Nelson, X. Li, N. J. Long and J. R. Durrant, *J. Am. Chem. Soc.*, 2004, **126**, 5225.
5. B. C. O'Regan, K. Bakker, J. Kroeze, H. Smit, P. Sommeling and J. R. Durrant, *J. Phys. Chem. B*, 2006, **110**, 17155.
6. N. W. Duffy, L. M. Peter, R. M. G. Rajapakse and K. G. U. Wijayantha, *Electrochem. Commun.*, 2000, **2**, 658-662.
7. M. Bailes, P. J. Cameron, K. Lobato and L. M. Peter, *J. Phys. Chem. B*, 2005, **109**, 15429-15435.